Journal of Magnetism and Magnetic Materials 469 (2019) 456–460

Contents lists available at ScienceDirect

Journal of Magnetism and Magnetic Materials

journal homepage: www.elsevier.com/locate/jmmm

Research articles

3D-printing of novel magnetic composites based on magnetic nanoparticles and photopolymers

Norbert Löwa*, Josephine-Marie Fabert, Dirk Gutkelch, Hendrik Paysen, Olaf Kosch, Frank Wiekhorst

Physikalisch-Technische Bundesanstalt, Abbestr. 2-12, 10587 Berlin, Germany

ARTICLE INFO

Keywords:
Magnetic nanoparticles
Magnetic particle spectroscopy
Magnetic particle imaging
3D printing
Generative manufacturing
Magnetic composites

ABSTRACT

A fast and cost-effective way to manufacture complex 3D structures out of numerous materials is the technique of 3D-printing employing vat photopolymerization where a liquid photopolymer in a vat is selectively cured layer by layer under radiation with light. To improve mechanical as well as functional properties different types of fillers can be added to the photopolymer. However, when fillers are added particular attention must be paid according to the quality of the resulting part (e.g. sedimentation, homogeneity, processability) which creates the need for appropriate quality evaluation. The aim of our work was to test the feasibility of printing magnetic composites which consist of photopolymers embedded with MNP. These magnetic composites are intended to be used as long-term stable phantoms in magnetic particle imaging. To assist the development of this novel imaging modality phantoms of defined geometry and magnetic properties are mandatory. With 3D printing of magnetic composites, it is possible to advance the characterization of MPI scanners with defined, long-term stable magnetic composite phantoms and opens an elegant way to print complex structures that could resemble body-like parts containing defined amounts of MNP.

1. Introduction

Magnetic nanoparticles (MNP) are of great interest in bio- and nanomedicine as they offer numerous promising therapeutic and diagnostic methods being intensively researched. A diagnostic method for the visualization of the spatial distribution of MNP, called magnetic particle imaging (MPI), has recently been introduced. MPI offers the specific measurement of MNP without any background signals from diamagnetic tissue. For MPI research, long-term stable phantoms with defined geometry and MNP content are required to determine the achievable resolution, to emulate anatomical structures, for cross-comparison of MPI scanners or as fiducial markers to verify the spatial position of the body under analysis.

A fast and cost-effective way to manufacture complex 3D structures out of numerous materials (e.g. polymers or ceramics) is the technique of generative printing, or commonly called 3D-printing. This additive technique allows manufacturing of customized parts with complex shapes that have a voxel resolution (= smallest printable feature) in the micrometer range. Among other additive manufacturing processes, the vat photopolymerization provides the best results in terms of complexity and accuracy of resulting parts and components [1]. The process starts from a liquid photopolymer which is selectively solidified layer by layer under light radiation in a liquid vat. Using a digital micromirror device a whole photopolymer layer can be irradiated and cured within a few seconds. Thus, 3D printed polymers already have found potential applications in aerospace [2,3], architecture [4], arts [5], and medical fields [6,7] with rather modest demands on the mechanical strength of the printed parts. To improve mechanical as well as functional properties, or even to introduce some new ones (e.g. mechanical, optical, electrical) many different fillers added to photopolymers have been tested [8]. Even MNP deposited on microfibers have been reported as fillers. Here, these fillers act as programmable reinforcement fibers oriented by external magnetic fields [9]. However, if fillers are added to a polymer, attention must be paid particularly to sedimentation phenomena, homogeneous dispersion, or alteration of the processability of the desired part.

The aim of our work was to investigate the feasibility of printing magnetic composites which consist of photopolymers embedded with MNP for manufacturing of sophisticated MPI phantoms. To this end, we developed a protocol for systematic quality evaluation of 3D-printed magnetic composites to generate complex, long-term stable MPI phantoms with defined magnetic properties (MNP amount per voxel,

* Corresponding author.
E-mail address: norbert.loewa@ptb.de (N. Löwa).

https://doi.org/10.1016/j.jmmm.2018.08.073
Received 20 June 2018; Accepted 25 August 2018
Available online 05 September 2018
0304-8853/ © 2018 The Authors. Published by Elsevier B.V. This is an open access article under the CC BY-NC-ND license (http://creativecommons.org/licenses/BY-NC-ND/4.0/).

signal shape per voxel). Prior to the actual 3D-printing, essential parameters such as magnetic properties of basic materials, homogenization procedure, mixture ratio, polymer cross-linking, and long-term stability were characterized and optimized to improve the quality of the resultant mixture. To magnetically characterize the liquid and solidified photopolymers with embedded MNP, we measured the quasi-static and dynamic magnetization behavior by means of dc-magnetometry (M − H) and Magnetic Particle Spectroscopy (MPS), respectively. To analyze the formability and smallest printable feature of a 3D-printed magnetic composite an appropriate geometry demonstrator was developed which also considers the orientation of different structures with respect to the printing direction. Finally, preliminary MPI imaging measurements of magnetic composites with different geometries were conducted.

2. Materials and methods

2.1. Magnetic nanoparticles

We used two commercially available MNP types, namely Ferucarbotran (Meito Sangyo, JPN) as well as EFH3 (FerroTec, USA). Ferucarbotran (FCT) is an aqueous suspension of iron oxide nanoparticles coated with carboxydextran consisting of single and multi-core MNP. In contrast, EFH3 is a light hydrocarbon oil-based ferrofluid usually used for audio speaker applications.

2.2. Photopolymers

In our experiments two types of photopolymers were used. E-shell 600 clear (E-Shell) and ABS 3SP Tough (ABS) are both light curing resins supplied by EnvisionTEC (Germany).

The clear E-Shell was specially designed for applications in the hearing aid industry (CE certified and Class-IIa biocompatible according to ISO 10993) and consists of 60–80% acrylic resin, 5–20% Urethane dimethacrylate, 10–25% Tetrahydrofurfuryl methacrylate and less than 1% Diphenyl (2,4,6-trimethylbenzoyl) phosphine oxide, with a density of 1185 g/L. The liquid material cures under UV light with a light intensity value of 230 mW. The indicated minimal resolution in z direction is 100 µm.

The ABS photopolymer is a very tough 3D printing material intended for applications where high stress and force resistance is required (e.g. automotive prototypes and consumer goods). The white liquid material is composed of 15–35% acrylated monomer, 10–40% methacrylated oligomer, 20–30% acrylated oligomer, 5–15% hexane-1,6-diol diacrylate, 1–3% isobornyl acrylate and 0.1–0.2% titanium dioxide having a density of 1185 g/L. The viscous material cures under UV light with a light intensity of 180 mW. The indicated minimal resolution in z direction is 50 µm.

To prepare the mixture of MNP (FCT, EFH3) and photopolymers (E-Shell, ABS) the desired volume fraction of MNP were added to the photopolymer. Best results according to stability and homogeneity of the mixture were obtained when sonicating the photopolymer during the addition of MNP using an ultrasound sonifier (UP200Ht, Hielscher Electronics, Germany). Finally, the magnetic photopolymer was degassed in an ultrasound bath (Bandelin, Germany). This prevents defects during the 3D printing process. As recommended by EnvisionTEC, the whole parts were post-cured after 3D printing in an incubator (Otoflash G171, Dentona, GER) to improve the cross linkage and ensure high durability of the parts.

2.3. 3D printing device

For printing of composite samples, a commercial 3D printer (Perfactory DSP XL) from EnvisionTEC with an indicated minimal (lateral) *xy* resolution of 42 µm was used (projector resolution 1920 × 1200 pixels). The *z* resolution is mainly material dependent and indicated within between 25 µm and 150 µm. The maximum build envelope has a size of 192 mm × 120 mm × 180 mm.

Custom made cylinders to fit into the sample holder of both magnetic characterization devices (MPS, M − H) of magnetic composites were 3D printed in quintuplicate. Were appropriate, data are presented as mean ± standard deviations with a coverage factor of $k = 1$ (i.e. a confidence level of about 68%).

2.4. Magnetic particle Spectroscopy (MPS)

To magnetically characterize the 3D printed magnetic composites according to homogeneity, long-term stability, and suitability for MPI we measured the non-linear magnetic susceptibility of the samples using a commercial Magnetic Particle Spectrometer (MPS-3, Bruker, Germany). During Magnetic Particle Spectroscopy (MPS) a sinusoidal excitation field amplitude $B = 25$ mT at a frequency $f_0 = 25$ kHz is applied to an MNP sample. Due to the inherent non-linearity of the magnetization curve the measured response of the MNP contains odd multiples of f_0 (i.e. higher harmonics).

For the measurement of 3D printed cylindric samples a specially designed non-magnetic sample holder was used and placed in the pick-up coil of the MPS system. The induced magnetization of the MNP response in the coil is amplified after filtering the fundamental excitation frequency f_0. An averaging period of 10 s was recorded to improve the signal-to-noise ratio. After Fourier transformation the spectral components show distinct amplitudes A_n at odd multiples n of the excitation frequency f_0 (see Fig. 1). To determine the device noise floor and the uncertainty of the harmonic amplitudes MPS spectra of 100 blank samples were recorded and the standard deviation was calculated. The third harmonic amplitude A_3 showed a residual moment of $5{\cdot}10^{-12}$ Am^2 underlining the high sensitivity of the MPS device. As A_3 is directly proportional to the absolute MNP content it can be used for MNP quantification (see inset of Fig. 1). In contrast, the shape of the spectrum expressed by the ratio A_5/A_3 of fifth A_5 and third A_3 harmonic amplitude depends on the dynamic magnetic behavior of the MNP and constitutes an indicator for the resolution of the MNP sample in MPI. Therefore, FCT ($A_5/A_3 = 30.2\%$) with a higher A_5/A_3 ratio is expected

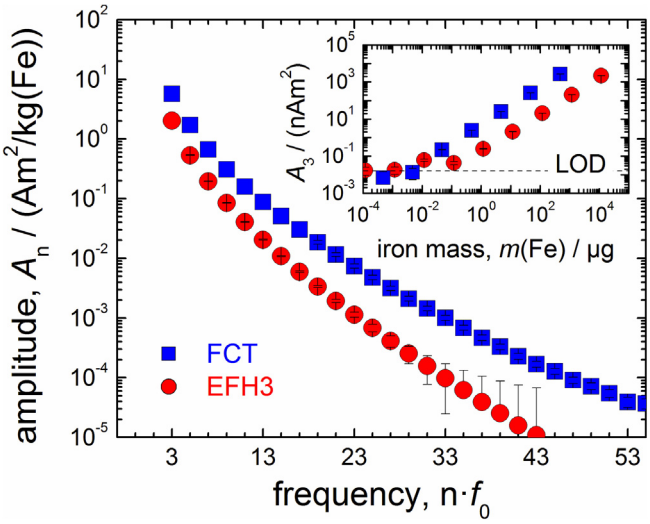

Fig. 1. MPS signal amplitudes A_n of FCT and EFH3 measured at 12 mT. The MPS signal amplitudes A_n were normalized to the respective iron amount of each sample. Inset: Serial dilutions of FCT and EFH3 in ddH_2O and mineral oil showing the linear relation of MPS signal amplitude A_3 and MNP amount (i.e. iron content). The horizontal line denotes the threefold standard deviation of 100 blank measurements and defines the apparent limit of detection (LOD). The shape of the MPS spectrum (also represented by the A_5/A_3 ratio) is not affected by dilution in the investigated dilution range. This indicates that the dynamic magnetic behavior of the MNP remains constant independent of dilution.

to perform better in MPI compared to EFH3 (A_5/A_3 = 26.1%).

2.5. DC-magnetometry (M − H)

The quasistatic magnetization M of the sample as a function of applied field strength H was measured at room temperature using a commercial magnetometer (MPMS XL, Quantum Design, USA). Therefore, the 3D printed cylinders were placed in a PE-straw sample holder. We determined the saturation magnetization at $H = 3.9{\cdot}10^6$ A/m, i.e. 5 T, as well as the initial mass susceptibility χ of the 3D printed samples and the raw MNP material. Additionally, from hysteresis loops between ± 5 T, the remanence M_r was determined.

2.6. Geometry demonstrator

To test the processability of the native photopolymers and the photopolymers with embedded MNP a geometric demonstrator was designed. The demonstrator consists of different elongated geometries (cylindrical as well as rectangular rods and tubes) arranged at different angles with respect to the printing direction (0°, 30°, 45°, and 90°). The geometries were designed with different sizes using a defined scaling scheme for each set of structure. The outer diameter d of the rods was varied from 0.1 mm up to 2 mm by scaling the length l = 10 d, proportionally. For the tubes the inner diameter d was varied in the same range as the diameter d of the rods. However, the wall thickness of each tube corresponds to the respective inner diameter d and the length l was scaled proportional: l = 20 d. Fig. 2 shows the CAD model of the final geometry. In addition to the rods and tubes, the demonstrator comprised rectangular solids and tubes as well as a thread-demonstrator which will not be analyzed in this work.

2.7. Magnetic particle imaging (MPI)

For analyzing the imaging perfomance of our phantoms, we used the commercial preclinical MPI scanner (MPI 25/20 FF Bruker BioSpin). This system is a field-free-point (FFP) scanner based on the system function approach for image reconstruction. For spatial encoding field gradients of 2.5 T/m in z-, and 1.25 T/m in x and y were used. For the measurement the FFP is moved on a closed 3D Lissajous-trajectory through the FOV by applying three orthogonal drive-fields of 12 mT amplitude oscillating at slightly different excitation frequencies (2.5 MHz divided by 102/96/99 in x-/y-/z-direction) and the MNP responses are acquired. For image reconstruction the additional measurement, the recording of the corresponding system function for each MNP type was accomplished. To this end, a tiny reference sample volume of MNP is placed by a robot at all chosen grid locations within the FOV of 25 mm × 25 mm × 13 mm and the resulting MNP responses during FFP trajectory cycles are collected. After background subtraction we used all components with an SNR threshold larger five. Images were obtained using the Kaczmarz algorithm with 15 iterations and a relative regularisation parameter of 0.01. To increase the overall sensitivity by +12 dB we used the recently developed separate receive coil gradiometrically minimizing the direct coupling of strong excitation fields into the receive chain of the MPI scanner.

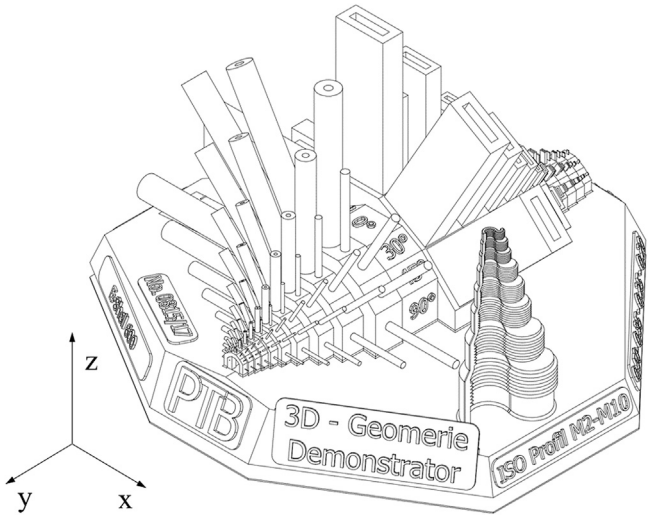

Fig. 2. CAD model of the geometry demonstrator designed to characterize the processability of photopolymers in 3D printing. The demonstrator comprises cylindrical (front part) as well as rectangular (rear part) rods and tubes. Each structure was designed to contain elements of several sizes and arranged at different angles (0°, 30°, 45°, and 90°) with respect to the printing direction z. In addition, a thread-demonstrator (M2–M10) was designed.

3. Results

3.1. Embedding of MNP in photopolymers

To test the impact of the homogenization procedure on the settling of embedded MNP we quantified the MNP concentration of the mixture (from the upper area) by taking 10 µL aliquots at different times after homogenization. The quantification was performed using MPS (at B = 25 mT). Fig. 3 shows the percentage decrease of quantified m(Fe) normalized to m(Fe) immediately after homogenization. We observed a significant settling of MNP (EFH3, FCT) over a period of 100 h if the mixture was merely stirred. In contrast, sonication (400 Ws) significantly reduced the MNP settling which results in a better homogeneity of the material during the 3D printing process (filled symbols in Fig. 3). Nevertheless, for time-consuming printing jobs of more than 10 h a concentration change of about 26% in the printed object should be considered. The printing of the following investigated samples took only some hours (estimated concentration change < 10%).

3.2. Magnetic characterization of 3D printed cylinders

We measured cylinders printed with different concentrations of MNP by means of MPS and M − H to determine the capability to generate samples with defined magnetic behavior that are characterized by both a linear scaling of magnetic moment with nominal MNP amount and a constant signal shape (i.e. unchanged properties).

For the dynamic magnetic behavior (MPS) a linear scaling of A_3 with nominal iron amount in the cylinders was observed (R^2 = 0.98) which is shown in Fig. 4 (left). Regarding the signal shape, expressed by A_5/A_3, no significant alteration with varying MNP amount was

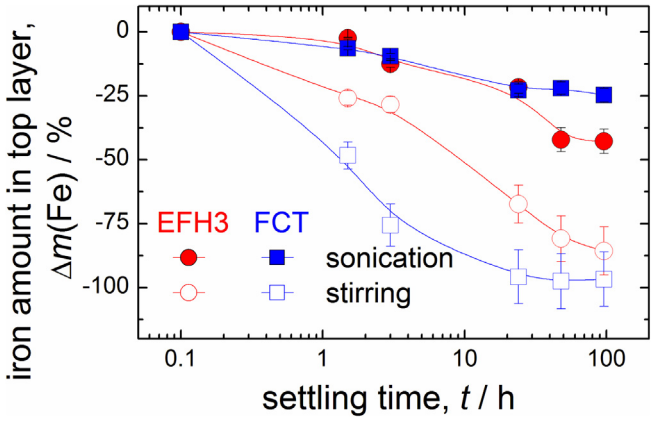

Fig. 3. Temporal change of iron amount (FCT and EFH3) in E-Shell measured in the top layer of 40 mL photopolymer-MNP mixture. The quantification was performed using MPS. The uncertainty bars indicate standard deviation from five aliquot samples.

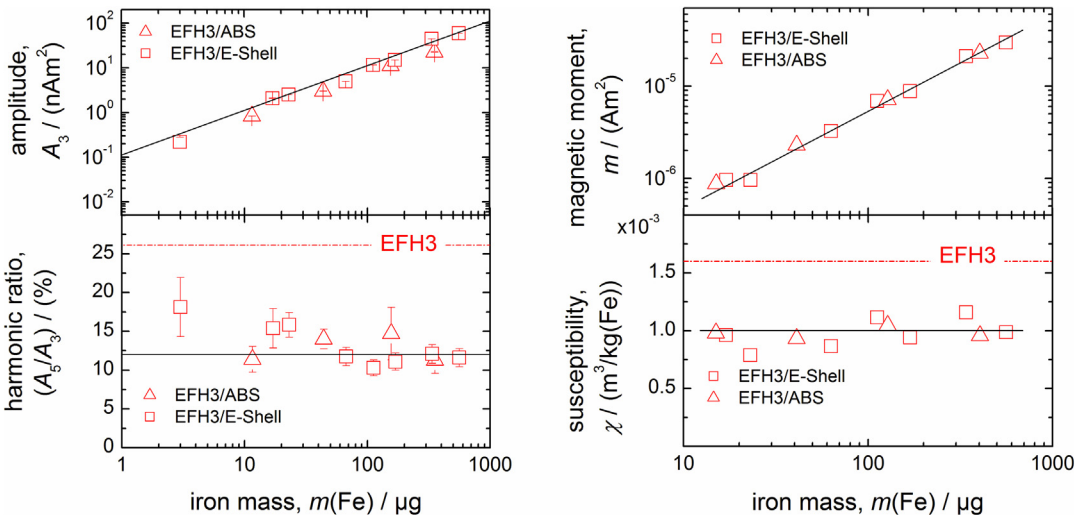

Fig. 4. Left: MPS measurements (B = 12 mT) on 3D printed cylinders with different concentrations of MNP (EFH3). A linear scaling of the third harmonic amplitude A_3 was observed (upper graph) whereas the signal shape factor $A_5/A3$ remained constant at 12% (lower graph). Right: M−H measurements on 3D printed cylinders with different concentrations of MNP (EFH3). A linear scaling of the magnetic moment at B = 5 T (upper graph) and unchanged mass susceptibility$\chi = 10^{-3}$ m^3/kg (Fe) (lower graph) with MNP amount was found. The uncertainty bars indicate standard deviation from five 3D printed samples.

observed.

Likewise for the static magnetic behavior of the 3D printed samples, the magnetic moment at B = 5 T scaled linearly with MNP amount (R^2 = 0.99) whereas the susceptibility χ remained constant. Similarly, the percentage remanence M_r compared to M_s was 1.9% and did not change with MNP amount.

For both, dynamic and static magnetic behavior, the signal shape (A_5/A_3, χ) changed significantly compared to the initial state of the raw MNP in liquid state (red dashed lines in Fig. 4). This can be explained by higher dipolar interactions and reduced mobility present in the solidified material compared to the liquid state.

3.3. Long-term stability

MPS was further used to analyze the long-term stability of the magnetic properties of the samples. Therefore, two samples with different MNP concentrations were measured over a period of 48 weeks and the percentage difference compared to the initial state directly after printing was determined. Fig. 5 shows the change of A_5/A_3 measured at B = 12 mT. We determined no (systematic) significant change of the dynamic magnetic behavior over the period of investigation.

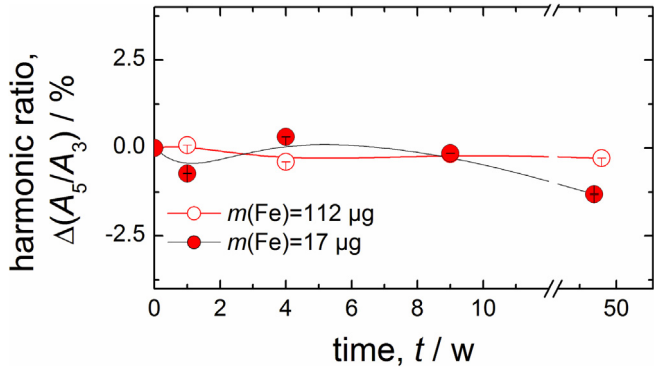

Fig. 5. Temporal change of MPS singal (spectral shape factor A_5/A_3) of 3D printed cylinders with different MNP amount. The uncertainty bars indicate standard deviation from five 3D printed samples.

3.4. Processability

The processability of the photopolymers (ES, ABS) without and with MNP (EFH3) was investigated by visual control of different elements (tubes, rods) as part of the 3D printed geometric demonstrator. Fig. 6 shows the 3D printed demonstrator without (a) and with (b) embedded MNP at a concentration of c(Fe) = 3.5 mg/mL in E-Shell. In this work, only two elements of the demonstrator, cylindrical rods and tubes, were analyzed. The summarized results of the visual control are displayed in Fig. 6c. Each bar covers the respective size range in which a structure was successfully formed.

We found, for the native photopolymers (white bars), that E-Shell covers the largest range of printable elements. Even rods with a diameter of only 0.1 mm were successfully formed whereas for ABS the minimal diameter was five times larger. Interestingly, for both materials, elements printed in horizontal direction are mostly of a lower quality compared to vertical or tilted orientations. In particular, horizontally printed tubes were not formed at all.

By adding MNP to photopolymers the quality of the elements of the demonstrator significantly improved (black bars). A clear improvement was observed for horizontally printed rods, resulting in a wider range of successfully printed elements. Additionally, for ABS, even smaller elements down to 0.25 mm are formed in vertical and tilted orientations after adding MNP.

3.5. Magnetic particle imaging

To assess the MPI performance of the 3D printed photopolymers, FCT and EFH3 were embedded in E-Shell with a resulting concentration of c(Fe) = 5.6 mg/mL. Finally, the liquid polymers were filled in a mask with the letters (P, T, and B). The lines of the letters had a thickness and depth of 1.5 mm and an overall length of 12 mm. The liquid polymers were light cured before each letter was scanned individually with MPI. As a reference, FCT was dispersed in demineralized water, filled in the mask of letters, and scanned with MPI as well.

Fig. 7 displays the lettering for FCT in water and E-Shell as well as EFH3 in E-Shell. In accordance with the MPS results in 3.2, the resulting resolution of the light cured phantoms had deteriorated in comparison to FCT in water. However, the structure of the phantom and the orientation of the lines are well visualized. Compared to FCT, the MPI image of the phantom with EFH3 in E-Shell is of slightly lower quality (stronger blurring, less resolution of details).

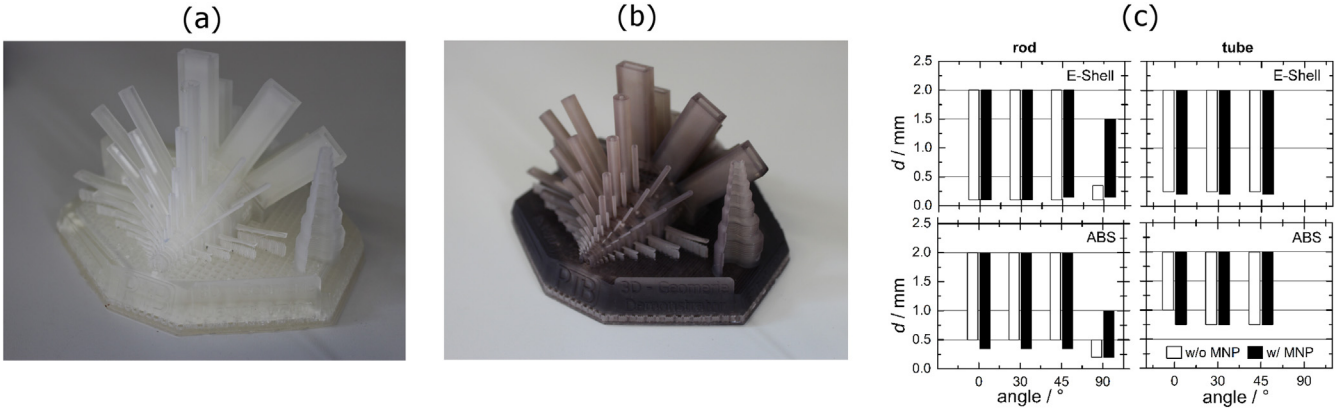

Fig. 6. 3D printed demonstrator using E-Shell without MNP (a) and with MNP (b) at a concentration of c(Fe) = 3.5 mg/mL. The evalution of the processability of two different photopolymers (E-Shell and ABS) with and without MNP (EFH3) was done by visual control of each structure. For each angle, with respect to the printing direction (0°, 30°, 45°, and 90°), the size range in which a successful formation was observed is covered by the bar (c).

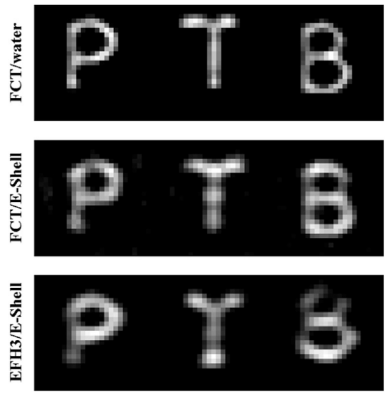

Fig. 7. MPI on magnetic composites arranged as letters (P, T, and B). Top: FCT dispersed in demineralized water. Middle: FCT embedded in E-Shell. Bottom: EFH3 embedded in EFH3.

4. Conclusions

In the present study we tested the feasibility of printing magnetic composites consisting of photopolymers with embedded MNP. Therefore, a protocol was developed to enable a systematic quality evaluation of 3D printed magnetic composites intended for use as MPI phantoms. We investigated key parameters such as magnetic properties of basic materials, homogenization procedure, mixture ratio, polymer cross-linking, long-term stability, and processability of the resulting parts in advance.

We finally printed magnetic composites of different MNP concentrations and found a linear scaling of the magnetic moment as well as unchanged magnetic properties with nominal iron amount which enables to produce MPI phantoms with defined magnetic signaling at different concentrations. As the printed magnetic composites were long term stable over weeks they are additionally suitable for calibration purposes, quality assurance as well as round robin test phantoms in MPI.

Furthermore, we developed a sophisticated demonstrator to analyze the formability and smallest printable feature of a 3D-printed magnetic composite which also considers the orientation of different structures with respect to the printing direction. This enabled a quantitative evaluation of the processability of magnetic composites. Interestingly, the quality of the elements of the demonstrator significantly improved for 3D printed magnetic composites compared to the photopolymer, alone.

Finally, the magnetic composites could be visualized by MPI properly which qualifies 3D printed magnetic composites for future MPI applications (e.g. as fiducial markers).

With the procedure developed here, it is possible to advance the characterization of the MPI scanner with defined, long-term stable magnetic composite phantoms. Finally, this opens an elegant way to print complex structures that could resemble body-like parts containing defined amounts of MNP.

Acknowledgments

This project was supported by the Federal Ministry of Economics and Technology within the TransMeT project “Magnetische Messtechnik für die Größenfraktionierung magnetischer Nanopartikel” and by Deutsche Forschungsgemeinschaft within the research grants “AMPI: Magnetic particle imaging: Development and evaluation of novel methodology for the assessment of the aorta in vivo in a small animal model of aortic aneurysms“ (grant SHA 1506/2-1) and “quantMPI: Establishment of quantitative Magnetic Particle Imaging (MPI) application oriented phantoms for preclinical investigations” (FKZ grant TR 408/9-1).

References

[1] Jeffrey W. Stansbury, Mike J. Idacavage, 3D printing with polymers: challenges among expanding options and opportunities, Dental Mater. 32 (1) (2016) 54–64, https://doi.org/10.1016/j.dental.2015.09.018.
[2] Eh.ud. Kroll, Dror Artzi, Enhancing aerospace engineering students' learning with 3D printing wind-tunnel models, Rapid Prototyp. J. 17 (5) (2011) 393–402, https://doi.org/10.1108/13552541111156522.
[3] Robert Bogue, 3D printing: the dawn of a new era in manufacturing? Assembly Automation 33 (4) (2013) 307–311, https://doi.org/10.1108/AA-06-2013-055.
[4] Hod Lipson, Melba Kurman, Fabricated: The new world of 3D printing, John Wiley & Sons, 2013.
[5] Carlo H. Séquin, Rapid prototyping: a 3d visualization tool takes on sculpture and mathematical forms, Commun. ACM 48 (6) (2005) 66–73, https://doi.org/10.1145/1064830.1064860.
[6] Fabian Rengier, et al., “3D printing based on imaging data: review of medical applications”, Int. J. Comput. Assisted Radiol. Surgery 5 (4) (2010) 335–341, https://doi.org/10.1007/s11548-010-0476-x.
[7] Sean V. Murphy, Anthony Atala, 3D bioprinting of tissues and organs, Nature Biotechnol. 32 (8) (2014) 773, https://doi.org/10.1038/nbt.2958.
[8] Xin Wang, et al., “3D printing of polymer matrix composites: a review and prospective”, Compos. Part B: Eng. 110 (2017) 442–458, https://doi.org/10.1016/j.compositesb.2016.11.034.
[9] J.J. Martin, B.E. Fiore, R.M. Erb, Designing bioinspired composite reinforcement architectures via 3D magnetic printing, Nat. Commun. 6 (2015) 641, https://doi.org/10.1038/ncomms9641 (2015).